J|A|C|S ARTICLES

Published on Web 11/05/2009

Mechanistic Investigations of Horseradish Peroxidase-Catalyzed Degradation of Single-Walled Carbon Nanotubes

Brett L. Allen,[†,||] Gregg P. Kotchey,[†] Yanan Chen,[†] Naveena V. K. Yanamala,[‡,§] Judith Klein-Seetharaman,[§] Valerian E. Kagan,[‡] and Alexander Star*[,†,||]

Departments of Chemistry, Environmental and Occupational Health, and Structural Biology, University of Pittsburgh, Pittsburgh, Pennsylvania 15260, and National Energy Technology Laboratory, Pittsburgh, Pennsylvania 15260

Received June 25, 2009; E-mail: astar@pitt.edu

Abstract: Single-walled carbon nanotubes (SWNTs) have been investigated for a variety of applications including composite materials, electronics, and drug delivery. However, these applications may be compromised depending on the negative effects of SWNTs to living systems. While reports of toxicity induced by SWNTs vary, means to alleviate or quell these effects are in small abundance. We have reported recently the degradation of carboxylated SWNTs through enzymatic catalysis with horseradish peroxidase (HRP). In this full Article, we investigated the degradation of both carboxylated and pristine SWNTs with HRP and compared these results with chemical degradation by hemin and $FeCl_3$. The interaction between pristine and carboxylated SWNTs with HRP was further studied by computer modeling, and the products of the enzymatic degradation were identified. By examining these factors with both pristine and carboxylated SWNTs through a variety of techniques including atomic force microscopy (AFM), transmission electron microscopy (TEM), Raman spectroscopy, ultraviolet−visible−near-infrared (UV−vis−NIR) spectroscopy, gas chromatography−mass spectrometry (GC−MS), high-performance liquid chromatography (HPLC), and liquid chromatography−mass spectrometry (LC−MS), degradation pathways were elucidated. It was observed that pristine SWNTs demonstrate no degradation with HRP incubation but display significant degradation when incubated with either hemin or $FeCl_3$. Such data signify a heterolytic cleavage of H_2O_2 with HRP as pristine nanotubes do not degrade, whereas Fenton catalysis results in the homolytic cleavage of H_2O_2 producing free radicals that oxidize pristine SWNTs. Product analysis shows complete degradation produces CO_2 gas. Conversely, incomplete degradation results in the formation of different oxidized aromatic hydrocarbons.

Introduction

Single-walled carbon nanotubes (SWNTs) have been at the forefront of nanoscience research for a variety of applications including gas sensing,[1−3] composite materials,[4,5] biosensing,[6−8] and drug delivery.[9−11] While the latter two applications have been successful, there are reports of cellular toxicity induced by SWNTs. Specifically, oxidative stress and the formation of free radicals,[12] robust inflammatory response,[13] and even asbestos-like pathogenicity[14] have been found as a result of the inception of SWNTs into biological systems. As a means to diminish these effects, various bioconjugation schemes have been used to functionalize SWNTs including DNA[15] and peptides,[16] as well as supramolecular approaches such as

[†] Department of Chemistry, University of Pittsburgh.
[‡] Department of Environmental and Occupational Health, University of Pittsburgh.
[§] Department of Structural Biology, University of Pittsburgh.
[||] National Energy Technology Laboratory.

(1) Kong, J.; Franklin, N.; Zhou, C.; Peng, S. S.; Cho, J. J.; Dai, H. *Science* **2000**, *287*, 622–625.
(2) Collins, P. G.; Bradley, K.; Ishigami, M.; Zettl, A. *Science* **2000**, *187*, 1801–1804.
(3) Kauffman, D. R.; Star, A. *Angew. Chem., Int. Ed.* **2008**, *47*, 6550–6570.
(4) Ajayan, P. M.; Schadler, L. S.; Giannaris, C.; Rubio, A. *Adv. Mater.* **2000**, *12*, 750–753.
(5) Zhu, J.; Kim, J.; Peng, H.; Margrave, J. L.; Khabashesku, V. N.; Barrera, E. V. *Nano Lett.* **2003**, *3*, 1107–1113.
(6) Allen, B. L.; Kichambare, P. D.; Star, A. *Adv. Mater.* **2007**, *19*, 1439–1451.
(7) Agüí, L.; Yáñez-Sedeño, P.; Pingarrón, J. M. *Anal. Chim. Acta* **2008**, *622*, 11–47.
(8) Kauffman, D. R.; Star, A. *Chem. Soc. Rev.* **2008**, *37*, 1197–1206.
(9) Bianco, A.; Kostarelos, K.; Prato, M. *Curr. Opin. Chem. Biol.* **2005**, *9*, 674–679.
(10) Kam, N. W. S.; Jessop, T. C.; Wender, P. A.; Dai, H. *J. Am. Chem. Soc.* **2004**, *126*, 6850–6851.
(11) Singh, R.; Pantarotto, D.; McCarthy, D.; Chaloin, O.; Hoebeke, J.; Partidos, C. D.; Briand, J.-P.; Prato, M.; Bianco, A.; Kostarelos, K. *J. Am. Chem. Soc.* **2005**, *127*, 4388–4396.
(12) Manna, S. K.; Sarkar, S.; Barr, J.; Wise, K.; Barrera, E. V.; Jejelowo, O.; Rice-Ficht, A. C.; Ramesh, G. T. *Nano Lett.* **2005**, *5*, 1676–1684.
(13) Lam, C.-W.; James, J. T.; McCluskey, R.; Arepalli, S.; Hunter, R. L. *Crit. Rev. Toxicol.* **2006**, *36*, 189–217.
(14) Poland, C. A.; Duffin, R.; Kinloch, I.; Maynard, A.; Wallace, W. A. H.; Seaton, A.; Stone, V.; Brown, S.; MacNee, W.; Donaldson, K. *Nat. Nanotechnol.* **2008**, *3*, 423–428.
(15) Kam, N. W. S.; O'Connell, M.; Wisdom, J. A.; Dai, H. *Proc. Natl. Acad. Sci. U.S.A.* **2005**, *102*, 11600–11605.
(16) Pantarotto, D.; Partidos, C. D.; Graff, R.; Hoebeke, J.; Briand, J.-P.; Prato, M.; Bianco, A. *J. Am. Chem. Soc.* **2003**, *125*, 6160–6164.

 10.1021/ja9083623 CCC: $40.75

functionalization with poly(ethylene glycol) (PEG).[17] These methods do, indeed, subdue the initial toxicity typically induced by this variety of carbon nanomaterials; however, the issue of long-term circulation without the possibility of physiological or even environmental degradation remains.

Recently, we have demonstrated the enzymatic degradation of carboxylated SWNTs using horseradish peroxidase (HRP) and low, localized concentrations of H_2O_2 ($\sim$40 μM).[18] Degradation of SWNTs with HRP was shown to proceed over the course of several weeks at 4 °C in the dark. The interaction between HRP and H_2O_2 has been extensively studied.[19] In essence, HRP, as a heme peroxidase, contains a single protoporphyrin IX heme group. While in an inactive form, the heme peroxidase is of a ferric (Fe^{3+}) oxidation state. Hydrogen peroxide then binds to the ferric species, and a transient intermediate forms, in which peroxide is bound to the heme iron as a ligand. It is then thought to undergo a protein-assisted conversion to an oxywater complex specifically through the His 42 and Arg 38 residues, leading to what is known as Compound I, comprised of a ferryl oxo iron (Fe^{4+}=O) and a porphyrin π cation radical. We hypothesize that the generation of Compound I (redox potential of 950 mV)[20] through the heterolytic cleavage of H_2O_2 would result in the degradation of carboxylated SWNTs located in close proximity to the HRP catalytic site. On the other hand, $FeCl_3$ would effect Fenton catalysis, where homolytic radical generation from H_2O_2 would demonstrate no selectivity, and pristine SWNTs would be degraded as well as carboxylated SWNTs.

To elucidate the mechanism of enzymatic degradation of SWNTs, we focus on the HRP preferential oxidation of carboxylated SWNTs over pristine SWNTs and the identification of the degradation products. From the perspective of the enzymatic substrate (SWNTs), it is tempting to speculate that, as a result of complete degradation, SWNTs will be completely oxidized to CO_2,[21] via formation of various intermediate species in the degradation solution. Additionally, from the perspective of HRP, it is unknown whether degradation is contingent upon proximity of the enzyme's heme site to the surface of SWNTs.

In this Article, the interaction between HRP and SWNTs is examined through a variety of methods including transmission electron microscopy (TEM), atomic force microscopy (AFM), ultraviolet−visible−near-infrared (UV−vis−NIR) spectroscopy, Raman spectroscopy, gas chromatography−mass spectrometry (GC−MS), high-performance liquid chromatography (HPLC), and liquid chromatography−mass spectrometry (LC−MS). As compared to our previous work, SWNTs were incubated with HRP and varying concentrations of H_2O_2 at higher temperature. Evaluation of these conditions shows significant acceleration of reaction kinetics at room temperature with little influence by an excess of H_2O_2 in the tested regime. These findings do not apply to pristine SWNTs, however, as no degradation was observed, alluding to hydrophobic interactions preventing proximity of the HRP heme site to the substrate (pristine SWNTs). Molecular modeling was additionally implemented to investigate possible binding sites for carboxylated and pristine SWNTs to HRP, resulting in varying proximity to this active site. Incubation with other ferric iron species including hemin and $FeCl_3$ with H_2O_2 resulted in the degradation of both carboxylated and pristine SWNTs, consistent with a homolytic cleavage of H_2O_2 and the formation of free radicals. Further characterization with GC−MS and HPLC of carboxylated SWNT samples (incubated with either HRP or ferric iron species) elucidated CO_2 production as expected, as well as multiple products in solution identified by LC−MS. Product analysis reveals the formation of CO_2 and intermediate oxidized aromatic hydrocarbons. These findings are important for better understanding the exact mechanism of enzymatic degradation of SWNTs.

Experimental Section

Materials. SWNTs prepared by the arc-discharge process[22] were purchased from Carbon Solutions, Inc. (P2-SWNT). Lyophilized HRP type VI, PBS, reagent grade MeOH, hemin (chloride), $FeCl_3$ (hexahydrate), and 30% H_2O_2 were purchased from Sigma Aldrich. Amplex Red was purchased from Molecular Probes, Invitrogen.

Carboxylation of SWNTs. SWNTs were carboxylated as reported previously.[23] Briefly, approximately 25 mg of SWNTs was sonicated (Branson 1510, frequency 40 kHz) in 200 mL of H_2SO_4/H_2O_2 (30%) at a ratio of 3:1 for 24 h at 0 °C. It is important to note that this solution is highly oxidizing. Caution must be taken when handling this system. After 10 and 15 h, 2.0 mL of H_2O_2 was supplemented into the reaction to compensate for H_2O_2 decomposition. The final dispersion was heated at 70 °C for 10 min, and subsequently diluted 10-fold, filtered on a 0.22 μm Teflon membrane filter, and washed with copious amounts of water to a neutral pH.

Incubation with HRP and H_2O_2. Two vials were prepared by sonicating for 1 min approximately 1 mg of carboxylated SWNTs into 4.0 mL of 1× (11.9 mM phosphates, 137 mM NaCl, and 2.7 mM KCl) phosphate buffered saline (PBS) per each vial. Lyophilized HRP type VI was solubilized in PBS at 0.385 mg/mL and added to the carboxylated SWNTs suspension at a volume of 4.0 mL, creating a total volume of 8.0 mL. All vials were then sealed with a septum and wrapped with parafilm to create an airtight seal. Following one full day of incubation, an initial 8 mL of either 80 or 800 μM H_2O_2 was added by needle through the septum to start the degradation reaction, followed by daily additions of 250 μL of either 80 or 800 μM H_2O_2 added to one of the two vials. This was continued on a daily basis for 10 days.

Monitoring HRP Activity with Amplex Red. Two vials were prepared by sonicating for 1 min approximately 1 mg of pristine SWNTs into 4.0 mL of PBS per each vial. Lyophilized HRP type VI was solubilized in PBS at 0.385 mg/mL, and then added to the two pristine vials at a volume of 4.0 mL, for a total volume of 8.0 mL per vial. An additional 8.0 mL of 80 μM H_2O_2 or 800 μM H_2O_2 was added to vials containing pristine SWNTs and HRP to start the degradation reaction. On a daily basis, 250 μL of either 80 or 800 μM H_2O_2 was injected into one of the two vials for 10 days. As a control, two vials consisting of 4.0 mL of HRP and 4.0 mL PBS were prepared, and the reaction was initiated by 8.0 mL of H_2O_2 (80 or 800 μM). Daily additions of

(17) Liu, Z.; Sun, X.; Nakayama-Ratchford, N.; Dai, H. *ACS Nano* **2007**, *1*, 50–56.
(18) Allen, B. L.; Kichambare, P. D.; Gou, P.; Vlasova, I. I.; Kapralov, A. A.; Konduru, N.; Kagan, V. E.; Star, A. *Nano Lett.* **2008**, *8*, 3899–3903.
(19) Filizola, M.; Loew, G. H. *J. Am. Chem. Soc.* **2000**, *122*, 18–25.
(20) Hayashi, Y.; Yamazaki, I. *J. Biol. Chem.* **1979**, *254*, 9101–9106.
(21) Schreiner, K. M.; Filley, T. R.; Blanchette, R. A.; Bowen, B. B.; Bolskar, R. D.; Hockaday, W. C.; Masiello, C. A.; Raebiger, J. W. *Environ. Sci. Technol.* **2009**, *43*, 3162–3168.
(22) Journet, C.; Maser, W. K.; Bernier, P.; Loiseau, A.; Lamy de la Chapelle, M.; Lefrant, S.; Deniard, P.; Lee, R.; Fischer, J. E. *Nature* **1997**, *388*, 756–758.
(23) Wei, Z.; Kondratenko, M.; Dao, L. H.; Perepichka, D. F. *J. Am. Chem. Soc.* **2006**, *128*, 3134–3135.

250 μL of either 80 or 800 μM H_2O_2 was performed for 10 days. All samples were then analyzed at days 1 and 10.

Amplex Red (Molecular Probes, Invitrogen) was employed to test HRP activity. A 10 mM stock solution of Amplex Red was prepared by dissolving the reagent in dimethyl sulfoxide (DMSO). To a 250 μL aliquot of sample being tested for enzymatic activity were added 234 μL of double-distilled water, 15 μL of 800 μM H_2O_2, and 1 μL of 10 mM Amplex Red. After gentle mixing, the UV−vis spectrum of the sample was taken with double-distilled water used as the background.

Incubation with Hemin and H_2O_2. Two vials were prepared by sonicating for 1 min approximately 1 mg of carboxylated or pristine SWNTs into 4.0 mL of dimethylformamide (DMF). Hemin (1×10^{-4} M in DMF) was then added in excess at a volume of 16.0 mL. Following 24 h of incubation, samples were centrifuged for 1 h and decanted of nonphysisorbed hemin,[24] followed by washing with double-distilled H_2O. The washed precipitates were then sonicated for approximately 1 min into 4.0 mL of double-distilled water followed by the addition of 4.0 mL of 800 μM H_2O_2 to initiate the reaction. Approximately 250 μL of 800 μM H_2O_2 was thereafter added on a daily basis.

Incubation with $FeCl_3$ and H_2O_2. Two vials were prepared by sonicating for 1 min approximately 1 mg of carboxylated or pristine SWNTs into 4.0 mL of double-distilled water. $FeCl_3$ (1×10^{-4} M aqueous) was then added at a volume of 500 μL and left to incubate for 24 h. Following incubation, 4.0 mL of 800 μM H_2O_2 was added to initiate the reaction. Approximately 250 μL of 800 μM H_2O_2 was then added on a daily basis.

Transmission Electron Microscopy. Samples in PBS solution were first centrifuged at 3400 rpm for 3 h and decanted of supernatant to effectively remove salts from the buffer. Resuspension into approximately 1 mL of DMF was performed by sonication for 1 min. One drop of the suspended sample was placed on a lacey carbon grid (Pacific-Grid Tech) and allowed to dry in ambient conditions for 2 h prior to TEM imaging (FEI Morgagni, 80 keV or JEOL 2100F, 200 keV). Samples in double-distilled water were used without any further preparation.

UV−vis−NIR Spectroscopy. Aqueous samples (150 μL) were analyzed using a Lambda 900 spectrophotometer (Perkin-Elmer) and 0.20 mL quartz cuvettes (path length: 1 cm, World Precision Instruments, Inc.). SWNTs were scanned from 600 to 1300 nm, while studies involving Amplex Red were scanned from 300 to 800 nm. All samples were used without any further treatment or purification.

Raman Spectroscopy. Samples were centrifuged at 3400 rpm for 3 h and decanted of supernatant to remove salts from the buffer, then resuspended in MeOH through sonication for approximately 1 min. Samples suspended in MeOH were prepared by drop-casting approximately 20 μL on a quartz microscope slide and drying. All spectra were collected on a Renishaw inVia Raman microscope using an excitation wavelength of 633 nm. Samples were scanned from 1000 to 1800 cm^{-1} to visualize D and G band intensity changes from the degradation process. Spectra were collected with a 15 s exposure time and averaged across 5 scans per sample.

Gas Chromatography−Mass Spectrometry (GC−MS). Approximately 2 μL of sample headspace (total headspace volume: 5 mL) was injected into a Shimadzu QP5050A GC-MS unit with an XTI-F capillary column by sampling through the septum of one of the two previously mentioned vials. A basic temperature program was performed, starting at 100 °C held for 1 min, followed by temperature ramping at a rate of 10 °C/min until a maximum temperature of 325 °C was achieved and held for an additional 10 min.

High-Performance Liquid Chromatography (HPLC). Samples in PBS solution or double-distilled water were first subjected to gentle heating (40 °C) under vacuum to remove water. Resuspension into approximately 200 μL of MeOH was performed by gentle shaking for 1 min, to concentrate the sample. A Waters 600 analytical HPLC system equipped with both a 996 photodiode array detector and 2410 refractive index detector was utilized for separation, and this device was outfitted with a reversed phase C18 column consisting of either a Waters Nova C18 or a Waters Symmetry 300 C18 column (Supporting Information). An isocratic solvent system consisting of 30% water and 70% MeCN was selected. Both the water and the MeCN were sparged with He (Valley Gas) for 30 min, and the C18 column was equilibrated for 30 min with the solvent prior to use. Twenty microliters of sample was analyzed over a period of 30 min with a solvent flow rate of 1 mL/min. Empower Pro software was utilized to complete all postprocess data analysis.

Liquid Chromatography−Mass Spectrometry (LC−MS). Approximately 3 mL of aqueous samples was acidified by the addition of 500 μL of 0.1 M HCl and extracted with dichloromethane (3 mL). After removal of dichloromethane, products were then redispersed in pure MeOH (500 μL). Approximately 10 μL of concentrated sample was injected into an Agilent/HP 1100 LC/MSD unit with an isocratic mobile phase of H_2O:MeCN (30:70) using an Xterra C18 column. Samples were analyzed for positive ions using electrospray mass spectrometry.

Atomic Force Microscopy (AFM). A Multimode scanning probe microscope (Veeco) was utilized in tapping mode for height, phase, and sectional analysis. Sample preparation was performed on freshly cleaved mica treated with approximately 20 μL of 0.1% (w/w) poly-L-lysine (aq) through spin-coating at 1400 rpm. Approximately 10 μL of sample (aq) was spin-coated at 1400 rpm and allowed to dry in ambient for 45 min prior to imaging. Using a "Supersharp" Si probe (tip radius <5 nm, AppNano), tapping mode at a drive frequency of 182.316 Hz, an amplitude set point of 0.2465 V, and a drive amplitude of 216 mV was performed. Images were initially scanned in a 13.1 μm area prior to magnification of relevant areas. Postimaging processing included section analysis for quantifying cross-sectional heights of samples.

Molecular Modeling, Docking of SWNTs to HRP. The 3-D structure of SWNTs was generated using Nanotube Modeler software[25] to have a diameter of 1.3 nm using the chiral indices (m, n) as (8, 8) and (14, 4) to model metallic and semiconducting SWNTs, respectively. SWNTs were modified to contain carboxyl and hydroxyl groups using the Builder Tool, provided by Pymol visualization software.[25] Docking of the modified (carboxylated and hydroxylated) and pristine SWNT to the HRP X-ray crystal structure (PDB ID: 1H5A, chain A) was performed using the iterated Local Search Global Optimization algorithm provided by AutoDock Vina.[26] The pdbqt format files (required as input) of both the receptor and the SWNT were generated using the ADT tools package provided by AutoDock4.0.[27] The entire surface of the target was searched for possible binding sites without bias. The grid maps representing the protein were calculated automatically by the AutoDock Vina software.[26] A cubic box was built around the protein with $126 \times 126 \times 126$ points as x, y, and z sizes. A spacing of 0.4 Å between the grid points was used, making the center of the protein to be the center of the cube, that is, x, y, and z centers at 5.766, 5.952, and 13.735, respectively. A total of two CPUs were used to perform the docking. All other parameters were set as default as defined by AutoDock Vina. We further analyzed these conformations to find the most preferred binding site (clusters with a maximum number of conformations and minimum energy) in each case. Although both binding sites were predicted as potential

(24) Kauffman, D. R.; Kuzmych, O.; Star, A. *J. Phys. Chem. C* **2007**, *111*, 3539–3543.

(25) DeLano, W. L. *The PyMOL Molecular Graphics System*; DeLano Scientific: Palo Alto, CA, 2002.

(26) Trott, O.; Olson, A. J. *J. Comput. Chem.*, DOI: 10.1002/jcc21334.

(27) Yanamala, N.; Tirupula, K. C.; Klein-Seetharaman, J. *BMC Bioinf.* **2008**, *9*, S16.

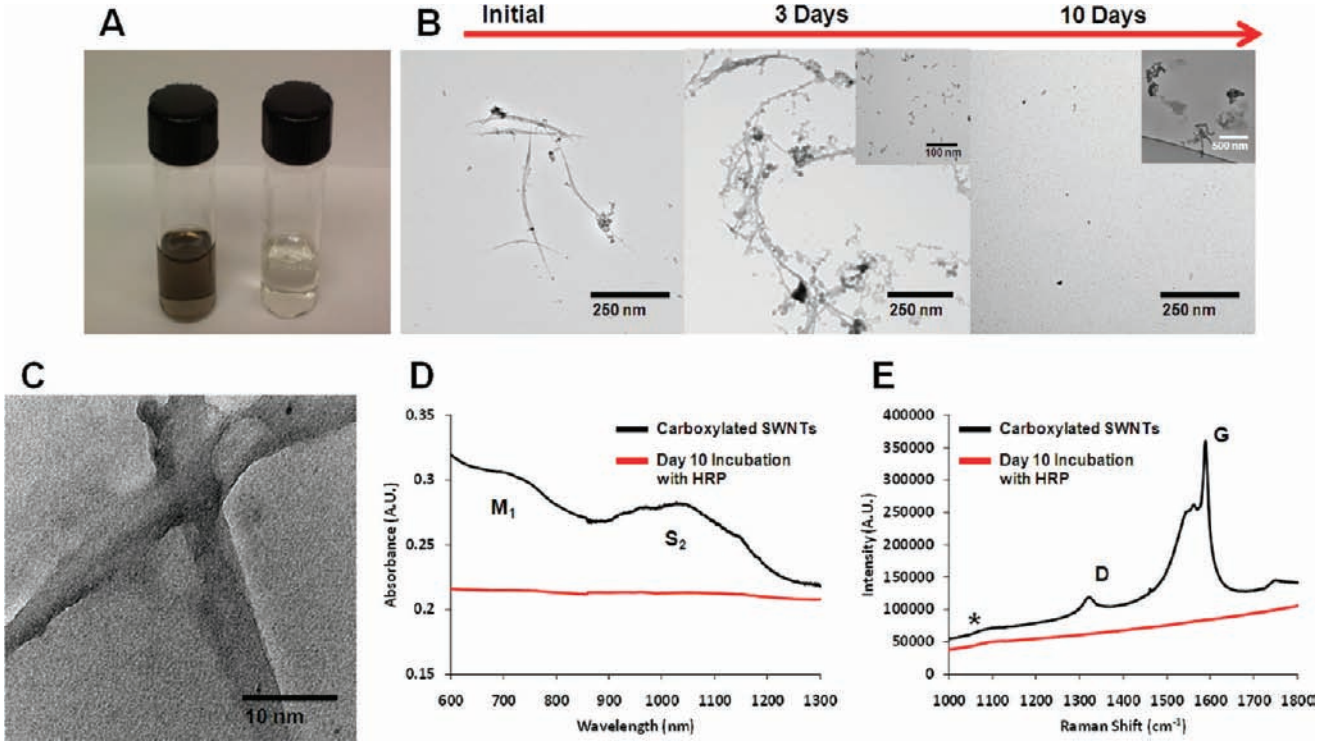

Figure 1. (A) Photograph demonstrating enzymatic degradation of carboxylated SWNTs (left) and after 10 days of incubation with HRP and H_2O_2 (right). (B) TEM micrograph confirming degradation of carboxylated SWNTs. (Insets) Approximately 2% of fields displayed carbonaceous intermediates. (C) High-resolution TEM micrograph of carboxylated SWNTs after 3 days of degradation with HRP and 80 μM H_2O_2. No crystal lattice structure is observed. (D) Vis−NIR spectra of carboxylated SWNTs (black) and HRP-degraded SWNTs (red). (E) Raman spectra of carboxylated SWNTs (black) and HRP-degraded SWNTs (red) (asterisk indicates contribution from quartz substrate).

interaction sites for modified (carboxylated and hydroxylated) SWNTs, the preference for each site differed.

Results and Discussion

Enzymatic Degradation of SWNTs at Room Temperature. In our previous communication, we presented evidence of enzymatic degradation of carboxylated SWNTs over the course of 12−16 weeks at refrigerated conditions (~4 °C).[18] It is known that rates of chemical reactions are generally increased by a factor of 2−4 for every 10 °C.[28] Thus, for a temperature increase from 4 to 25 °C, an increase in the kinetic rate by a factor of 4−8 should be observed. Such an increase in temperature would result in the same degradation in approximately 2 weeks, provided that enzyme denaturation does not occur.

HRP and carboxylated SWNTs were statically incubated for 24 h at room temperature prior to the addition of 8.0 mL of 80 μM H_2O_2 to begin the reaction. H_2O_2 was then subsequently added to the reaction on a daily basis at 250 μL volume for 10 days, and the sample vials were kept in the dark to avoid photolysis of H_2O_2.[29] As evidence of degradation after 10 days of incubation, Figure 1A shows a photograph of an initial vial of carboxylated nanotubes (left) versus day 10 of incubation with HRP and daily additions of 80 μM H_2O_2 (right). There is a noticeable decrease in light scattering and absorbance from the sample at day 10 of incubation, alluding to degradation as witnessed previously over the course of 16 weeks.

To confirm that this decrease in light scattering was the result of degradation, transmission electron microscopy (TEM) was performed on samples prior to and after 10 days of incubation with HRP and H_2O_2. Figure 1B shows tracking of nondegraded, carboxylated SWNTs (left) and carboxylated SWNTs degraded by HRP and H_2O_2 at room temperature over the course of 10 days. As can be seen, carboxylated SWNTs display lengths of approximately 400 nm prior to incubation. After 3 days, some carbonaceous material is present resembling that of SWNTs. Additionally, Figure 1C shows a high-resolution TEM image of SWNTs after 3 days of degradation. As observed, while a one-dimensional structure is still evident, no tubular structure is present, indicating the oxidation of graphitic material. However, after 10 days, no noticeable carbon nanotube material is apparent, presumably due to the oxidation of the graphitic carbon lattice to CO_2 gas. While most fields on a lacey carbon TEM grid appeared to be unoccupied, ~2% (1 field in 50) had carbonaceous products, not resembling SWNTs (inset) and presumably represent an intermediate of incomplete oxidation.

Degradation was additionally confirmed spectroscopically. Visible−near-infrared (vis−NIR) absorption spectroscopy measurements were taken on carboxylated SWNTs (aq) and those degraded after 10 days of incubation with HRP and 80 μM H_2O_2 (aq). It should be noted that SWNTs are synthesized as mixtures of varying diameters and chiralities, exhibiting metallic and semiconducting electronic properties, as well as corresponding spectral features. Figure 1D shows the spectral features of carboxylated SWNTs, evident from the broad S_2 second semiconducting transition absorbing between 1000 and 1100 nm, and the M_1 metallic transition absorbing between 650 and

(28) Magazanik, L. G.; Vyskocit, F. *J. Physiol.* **1975**, *249*, 285–300.
(29) Hunt, J. P.; Taube, H. *J. Am. Chem. Soc.* **1952**, *74*, 5999–6002.

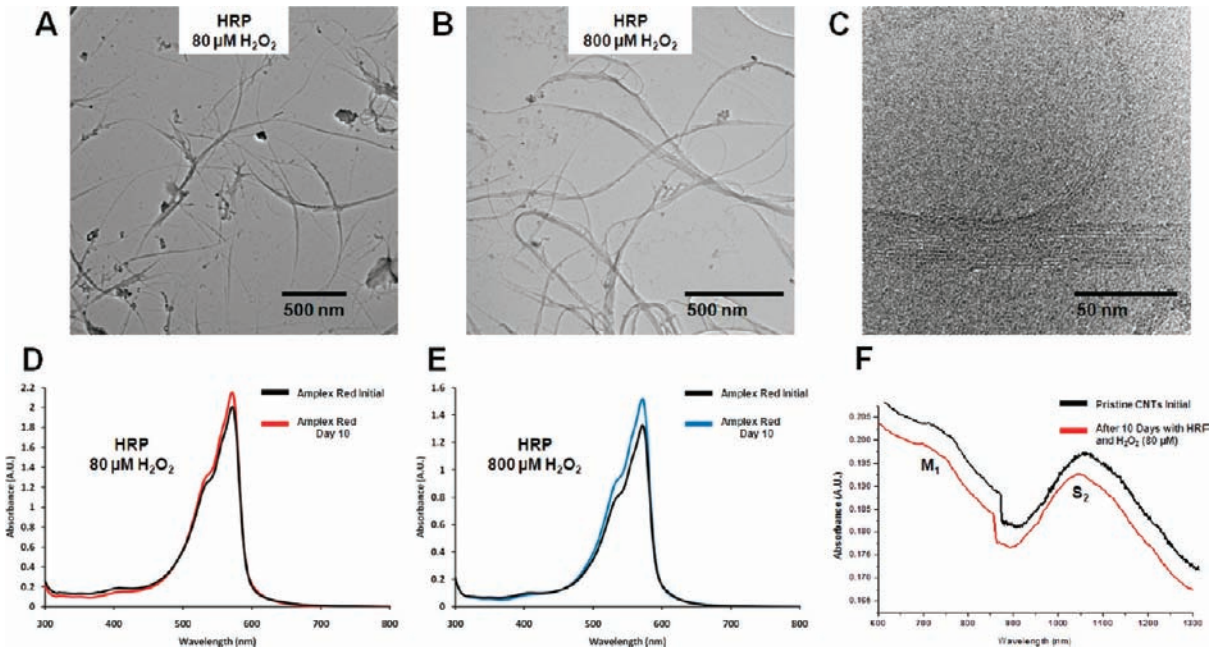

Figure 2. (A) TEM micrograph of pristine SWNTs after 10 days of incubation with HRP and 80 μM H_2O_2 and (B) 800 μM H_2O_2. (C) High-resolution TEM micrograph of pristine SWNTs after 10 days of degradation with HRP and 800 μM H_2O_2. Crystal lattice structure is observable as SWNTs appear bundled, with exfoliation of smaller bundles present at the immediate ends of larger bundles. (D) UV−vis spectra of Amplex Red activity with HRP and 80 μM H_2O_2 or (E) 800 μM H_2O_2. (F) Vis−NIR spectra of pristine SWNTs (black) and after 10 days of incubation with HRP and 80 μM H_2O_2.

750 nm.[30,31] These bands appear to be subdued upon incubation with HRP and H_2O_2 (red trace). As graphitic structure becomes oxidized, transitions associated with sp^2 carbon framework of pristine SWNTs would diminish and completely disappear as a result of enzymatic degradation. Further examination with Raman spectroscopy reveals similar results. Figure 1E displays the tangential G-band and disorder-induced D-band of carboxylated SWNTs, as previously reported.[32] After enzymatic degradation for 10 days, these bands are no longer present, and only the signal for the quartz substrate (denoted by *) is present. These data again confirm the degradation of carboxylated SWNTs over the span of 10 days when incubating at room temperature (25 °C).

To examine further the mechanism of degradation between HRP and SWNTs, studies were performed investigating the role of carboxylated versus pristine graphitic lattices. As such, pristine SWNTs (Carbon Solutions, Inc.) were incubated under the same conditions as mentioned for carboxylated SWNTs. Briefly, pristine SWNTs were sonicated for approximately 5 min in DMF. Subsequently, samples were centrifuged at 3400 rpm, and the supernatant was decanted. The precipitated pristine SWNTs were then washed with double-distilled H_2O and resuspended in 4.0 mL of PBS through additional sonication. Pristine SWNTs treated in this manner retained some solubility (suspension stable for up to 2 days), but not to the extent of carboxylated SWNTs. Periodic shaking was then necessary to resuspend pristine SWNTs. To this suspension was added 4.0 mL of 0.385 mg/mL HRP (aq), and it was allowed to incubate for 24 h prior to H_2O_2 additions as previously performed. Over the course of the 10 day incubation with HRP and H_2O_2, there was no noticeable decrease in scattering or absorbance but increased aggregation, suggesting a lack of degradation of carbon material. To confirm this phenomenon, TEM imaging was performed on an aliquot taken 10 days after incubation with HRP and 80 μM H_2O_2. Figure 2A shows that pristine SWNTs are still intact (1−2 μm in length) and do not appear to be deformed or degraded in any manner. Because pristine SWNTs did not degrade, two factors were of immediate importance to investigate: (1) the role of H_2O_2 concentration and (2) the viability of HRP with pristine SWNTs.

Pristine SWNTs were then subjected to conditions identical to those mentioned with the exception of initiating degradation with an excess of 800 μM H_2O_2 (K_M: 0.11 mM).[33] It was interesting to see whether changing the concentration by an order of magnitude would affect the degradation of pristine SWNTs in a significant manner. As indicated by the TEM micrograph in Figure 2B, no significant degradation was found with the addition of 800 μM H_2O_2. Closer examination using high-resolution TEM revealed bundled SWNTs that retained their crystal lattice structure after 10 days of incubation with HRP and 800 μM H_2O_2 (Figure 2C). Such data, however, may point to the denaturation or inactivation of HRP by pristine SWNTs. It is then advantageous to investigate whether the enzyme retains activity in solution with pristine SWNTs and if this activity is affected by the 10-fold increase in H_2O_2 concentration.

To test the viability of HRP in the presence of pristine SWNTs, Amplex Red was used. Amplex Red (10-acetyl-3,7-dihydroxyphenoxazine) is a reagent commonly employed to measure trace H_2O_2 concentrations in biological systems.[34] In the presence of H_2O_2, Amplex Red undergoes HRP-catalyzed oxidation to form radical intermediates. The radical intermedi-

(30) Hamon, M. A.; Itkis, M. E.; Niyogi, S.; Alvaraez, T.; Kuper, C.; Menon, M.; Haddon, R. C. *J. Am. Chem. Soc.* **2001**, *123*, 11292–11293.
(31) The first semiconducting transition (S1) is expected between 1800 and 1900 nm; however, water absorbs strongly in this regime, masking any features attributed to this transition.
(32) Dresselhaus, M. S.; Dresselhaus, G.; Jorio, A.; Souza Filho, A. G.; Saito, R. *Carbon* **2002**, *40*, 2043–2061.
(33) Gilabert, M. A.; Fenoll, L. G.; García-Molina, F.; Tudela, J.; García-Cánovas, F.; Rodríguez-López, J. N. *Biol. Chem.* **2004**, *385*, 795–800.
(34) Gorris, H. H.; Walt, D. R. *J. Am. Chem. Soc.* **2009**, *131*, 6277–6282.

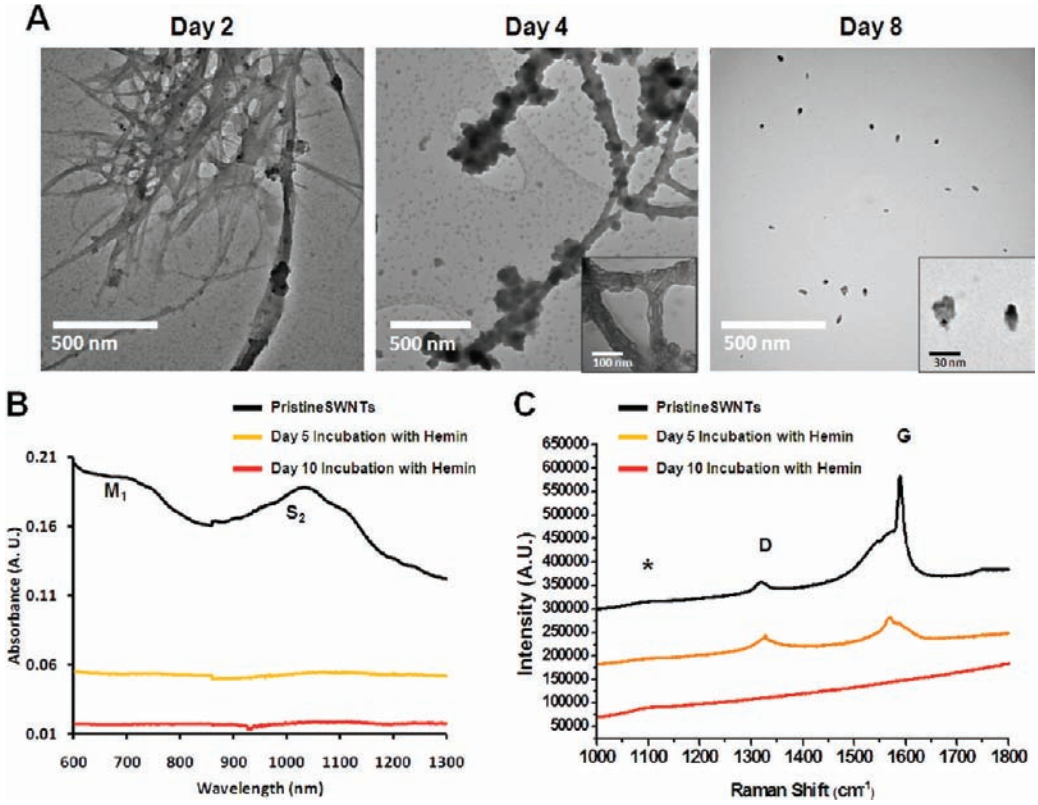

Figure 3. (A) TEM micrographs displaying degradation of pristine SWNTs with hemin and 800 μM H_2O_2 over 10 days. Inset at day 4 shows deformation of individual fibers, while inset at day 8 shows residual iron. (B) Vis−NIR spectra of pristine SWNTs after incubation with hemin and H_2O_2. (C) Raman spectra of pristine SWNTs degraded by hemin and H_2O_2. (Asterisk indicates quartz substrate contribution.)

ates then proceed via a dismutation reaction to form resorufin, which has distinct fluorescence and absorbance spectra. Because the conversion of Amplex Red to resorufin depends on an active enzyme, the spectral features of resorufin can be used to monitor HRP activity. Thus, by monitoring an absorbance peak present at 570 nm, a result of resorufin produced from active enzyme and Amplex Red, it is possible to validate enzyme viability. Figure 2D,E depicts the results for the Amplex Red assay; three major trends can be ascertained from this data. First, initially, the UV−vis spectroscopic data displayed a peak around 570 nm, which indicated that HRP was originally active. Second, there was no decrease in absorbance at day 10; therefore, a sufficient quantity of HRP remained active to catalyze the conversion of Amplex Red into resorufin. While it may be possible that HRP is deactivated by auto-oxidation, a significant contribution from active HRP is still present. Third, HRP remained viable after additions of both 80 and 800 μM H_2O_2. These observations logically lead one to conclude that while HRP remains active (or active in part) in the presence of pristine SWNTs, it cannot catalyze their degradation in the tested time frame and given HRP concentration. Further spectroscopic confirmation of this phenomenon was observed using vis−NIR spectroscopy. Figure 2F shows a spectroscopic comparison between pristine SWNTs and those subjected to HRP and 800 μM H_2O_2. As indicated by the spectral features, characteristic S_2 and M_1 bands are present after 10 days of incubation, demonstrating a lack of degradation. One plausible explanation for this observation involves interactions between SWNTs and HRP, to be discussed below.

Oxidation of SWNTs by Fenton's Reagents. Data thus far allude to heterolytic cleavage of H_2O_2 to form Compound I and H_2O. As pristine SWNTs do not degrade in the presence of HRP and H_2O_2, this lends credibility to a proximity effect between the active site of Compound I and SWNTs. In contrast to this mechanism, homolytic cleavage of H_2O_2 results in the production of hydroxyl radicals ($^{\bullet}OH$) via Fenton's chemistry.[35] In essence, H_2O_2 oxidizes Fe^{2+} to Fe^{3+} and produces OH^- and $^{\bullet}OH$. Ferric iron is then reduced back to ferrous iron by additional peroxide, producing H^+ and $^{\bullet}OOH$.

$$Fe^{2+} + H_2O_2 \rightarrow Fe^{3+} + {}^{\bullet}OH + OH^- \quad (1)$$

$$Fe^{3+} + H_2O_2 \rightarrow Fe^{2+} + {}^{\bullet}OOH + H^+ \quad (2)$$

While both Compound I and hydroxyl/hydroperoxyl radicals are highly oxidizing species, the ability of Compound I to degrade SWNTs may be contingent upon special proximity to the heme active site, whereas the reactivity of hydroxyl and hydroperoxyl radicals is limited only by the rate of diffusion and their half-lives.[36]

To compare the HRP oxidation mechanisms involving Compound I formation and hydroxyl and hydroperoxyl radicals formed via Fenton chemistry to degrade SWNTs, we chose hemin (chloride), a ferric iron chloroprotoporphyrin, and a ferric iron salt ($FeCl_3$). It is important to note that while Fenton catalysis is typically initiated with ferrous iron, we chose ferric iron species to be consistent among all iron forms tested. Most importantly, because $FeCl_3$ lacks the protein structure of HRP, homolytic cleavage of H_2O_2 to form hydroperoxyl and hydroxyl

(35) Walling, C. *Acc. Chem. Res.* **1975**, *8*, 125–131.
(36) Yan, E. B.; Unthank, J. K.; Castillo-Melendez, M.; Miller, S. L.; Langford, S. J.; Walker, D. W. *J. Appl. Physiol.* **2005**, *98*, 2304–2310.

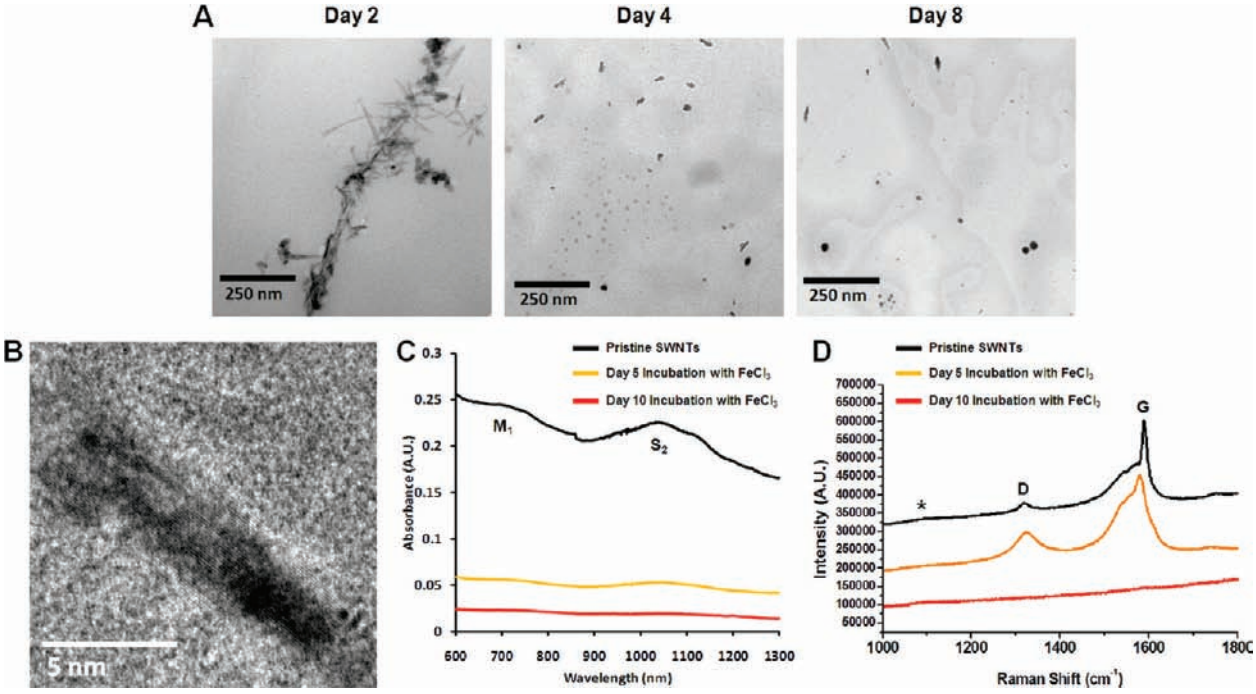

Figure 4. (A) TEM micrographs of $FeCl_3$-catalyzed degradation of pristine SWNTs. SWNTs are shown to "flake" at day 2, followed by progressive shortening through day 8. (B) High-resolution TEM micrograph of "flake" produced after degradation (day 5) with $FeCl_3$ and 800 μM H_2O_2. Crystal lattice structure is still observable for the individual flake. Further elemental analysis shows the presence of carbon, oxygen, and iron (Supporting Information). (C) Vis−NIR spectra of pristine SWNTs degraded by $FeCl_3$ and 800 μM H_2O_2. (D) Raman spectra of pristine SWNTs degraded by $FeCl_3$ and 800 μM H_2O_2. (Asterisk indicates quartz substrate contribution.)

radicals is the predominant pathway for oxidation to occur, whereas hemin may act under either a homo- or a heterolytic cleavage mechanism.

For the examination of hemin, approximately 1 mg of pristine or carboxylated SWNTs was sonicated in 4.0 mL of DMF. Hemin (1×10^{-4} M, in DMF) was then added in excess at a volume of 16.0 mL. After 24 h of incubation, samples were centrifuged, decanted of excess hemin and DMF, and sonicated into 4.0 mL of double-distilled water. Typically, hemin forms an inactive dimer when free in solution.[37] However, it has been previously shown that porphyrins physisorb onto SWNTs, providing close proximal contact to the iron site.[24] Such proximity may result in increased activity, generating oxidizing species close to carboxylated and pristine SWNTs, promoting degradation. The degradation reaction was initiated by the addition of 4.0 mL of 800 μM H_2O_2, followed by daily additions of 250 μL of 800 μM H_2O_2 for a total of 10 days.

Over the 10 day incubation period, carboxylated SWNTs were degraded by hemin and 800 μM H_2O_2 (Supporting Information). In contrast to incubation with HRP and 800 μM H_2O_2, pristine SWNTs have also showed significant degradation. Figure 3A shows TEM images of the products of this degradation reaction over the course of 10 days. As demonstrated, after 2 days of incubation, pristine SWNTs appeared to "swell" and aggregated together. After day 4, however, pristine SWNTs broke down with significant noticeable deformation. By day 8, only small carbonaceous products and residual iron (catalyst from nanotube synthesis) were present (Supporting Information).

Spectroscopic data further support these observations. Figure 3B shows the vis−NIR spectra of pristine SWNTs degraded with hemin and H_2O_2 over 10 days. A loss of intensity and changes in band shape for the M_1 and S_2 metallic and semiconducting transitions of pristine SWNTs are quite evident and comparable to results seen with carboxylated SWNT degraded by HRP and H_2O_2. These spectral changes suggest degradation of the pristine graphitic material. Raman characterization further supports this degradation as demonstrated in Figure 3C. Pristine SWNTs display prominent D and G band contributions initially. After 5 days of degradation, the D:G band ratio increases, indicating modification of the pristine SWNT structure, accompanied by an increase in the number of defect sites. By day 10 of incubation, only the residual peak for the quartz substrate is present, as indicated by an asterisk. Therefore, the degradation of pristine SWNTs by hemin is likely to proceed by increased proximity to the active iron site, whereas HRP limits this proximity as a result of distal site binding, as will be further explained.

To compare these degradation methods to that of a Fenton catalyst, where only free radicals are generated, $FeCl_3$ was used. Briefly, 1 mg of carboxylated (Supporting Information) or pristine SWNTs was sonicated for 1 min into 4.0 mL of double-distilled water. Next, 500 μL of $FeCl_3$ (1×10^{-4} M, aqueous) was added to all samples, and they were incubated for 24 h before 4.0 mL of 800 μM H_2O_2 was added to initiate the reaction. Daily additions of 250 μL of 800 μM H_2O_2 were continued for 10 days. Figure 4A shows the TEM images of pristine SWNTs incubated with $FeCl_3$ and H_2O_2. Evidently, even after 2 days of incubation, long pristine SWNTs oxidized into individual flakes, an observation similar to that reported by Kosynkin et al. whereby unzipping was facilitated by chemical treatment with H_2SO_4 and $KMnO_4$.[38] By day 4, flakes were approximately 40 nm in length, while at day 8, it appeared that mostly residual iron was present. Upon closer examination with

(37) Nakamoto, K. *Coord. Chem. Rev.* **2002**, *226*, 153–165.

(38) Kosynkin, D. V.; Higginbotham, A. L.; Sinitskii, A.; Lomeda, J. R.; Dimiev, A.; Price, K. B.; Tour, J. M. *Nature* **2009**, *458*, 872–876.

high-resolution TEM, flakes (~3 nm wide) displayed a crystalline structure, indicating the presence of graphitic material (Figure 4B).

Similar results were obtained spectroscopically, as well. Figure 4C shows the vis−NIR spectra of pristine SWNT degradation. Initially, pristine SWNTs displayed pronounced semiconducting and metallic transition bands (S_2 and M_1, respectively). Following 5 days of incubation, these bands were greatly suppressed, and finally all band structure was lost at day 10. Raman data conformed to these results as shown in Figure 4D. Pristine SWNTs were observed to have defined D and G band peaks contributed by the defect sites and the pristine graphitic lattice of the SWNTs, respectively. The ratio of the D to G bands then increased after 5 days, indicating progressive oxidation of the material. By day 10, however, only the peak for the quartz substrate was observed, indicating a complete loss of nanomaterial.

Results of both hemin and $FeCl_3$ demonstrate that by increasing the proximity of active iron sites and generating radical oxygen species, pristine SWNTs will degrade. Conversely, no degradation is evident with pristine SWNTs and HRP, indicating an alternate degradation mechanism, presumably because of the heterolytic cleavage of H_2O_2 to form Compound I. The role of SWNTs in the homolytic degradation reaction is even more significant as Fenton catalysis is typically generated from ferrous iron, although it is ferric prior to addition with pristine SWNTs. Because the degradation reaction does progress, it may be that carbon nanotubes are acting as a reducing agent to reduce ferric iron to ferrous iron because of their unique redox properties[39] and possible reducing character of the inherent polyphenol functionalities located within the SWNT lattice of both pristine and carboxylated varieties.[40]

Degradation Product Analysis. Identification of intermediate products of the HRP-catalyzed degradation reaction was performed using HPLC, LC−MS, and GC−MS. While the formation of CO_2 gas will be shown as a likely final product of the degradation process, classes of intermediate species resulting from incomplete degradation have yet to be identified or enumerated. It may be possible that multiple intermediate products may form and reside in the aqueous media, including various oxidized aromatic hydrocarbons. To begin evaluating the variety of species present within aqueous media, reversed-phase HPLC was implemented. Briefly, aqueous samples were dried by heating under vacuum at 40 °C for 2 h, thus retaining carbonaceous products and buffer salts contained therein. It is important to note that during this procedure it is possible that low boiling point molecules were lost in the process. However, in PBS solution prior to concentration, they are in low abundance and not detected by an HPLC chromatogram (Supporting Information). Reagent grade MeOH was then added to resuspend the dehydrated product through gentle shaking. Samples consisting of HRP-degraded, hemin-degraded, and $FeCl_3$-degraded, carboxylated nanotubes at day 8 of incubation were injected into a reversed phase HPLC column. An isocratic program consisting of a 30:70 mixture of H_2O:MeCN ran for 30 min at a flow rate of 1 mL/min. Figure 5A shows the resulting chromatogram from HRP-degraded SWNTs. Beginning at 4.5 min and terminating at 10.5 min, a series of peaks are

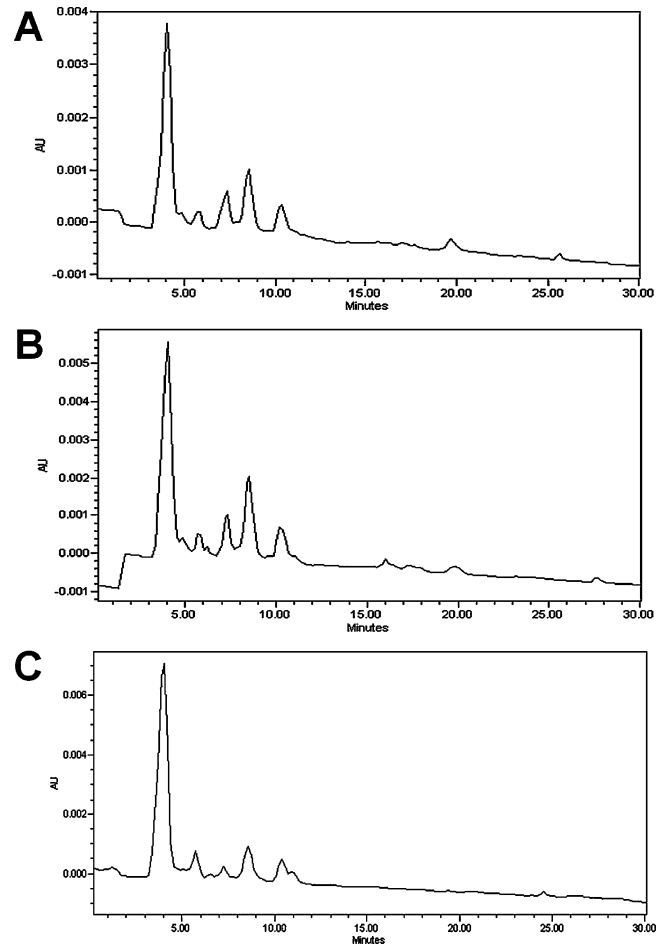

Figure 5. (A) HPLC (Nova C18 column) chromatogram of HRP-degraded, carboxylated SWNTs after 8 days of incubation. (B) Hemin-degraded and (C) $FeCl_3$-degraded, carboxylated SWNTs after 8 days of incubation.

eluted with a 1 min elution delay. This series of peaks may be due to the presence of oxidized aromatic hydrocarbons, while elution peaks at 20 and 25 min may be due to larger oxidized aromatic species with higher affinity to the C18 column. As a comparison, mellitic acid and *trans*-cinnamaldehyde were injected as standards (Supporting Information). They were observed to elute in the same retention time as peaks presented in the HRP-degraded sample. Additionally, pure HRP in MeOH was injected to verify that observed peaks from HRP-degraded samples did not belong to fragmented enzyme (Supporting Information).

Products resulting from hemin and $FeCl_3$ degradation by free radical oxidation were analyzed by HPLC. Figure 5B shows the resulting chromatogram for hemin degraded products. As is evident with hemin degradation, a series of peaks is observed immediately after 4.5 min, at elution times previously demonstrated for HRP products, and identified as possible oxidized aromatic hydrocarbons. Only past elution times of 15 min are any differences noted in the chromatograms (areas indicative of larger oxidized aromatic hydrocarbons). Similar results are shown for $FeCl_3$-degraded carboxylated SWNTs (Figure 5C). A series of peaks corresponding presumably to oxidized 2−5 membered rings is seen, although with less intensity. These results demonstrate that products formed are strikingly similar regardless of heterolytic or homolytic reaction pathways for SWNT degradation. However, differences present at elution times past 15 min, where larger oxidized polycyclic aromatic

(39) Duque, J. G.; Pasquali, M.; Schmidt, H. K. *J. Am. Chem. Soc.* **2008**, *130*, 15340–15347, and references cited therein.
(40) Kuznetsova, A.; Popova, I.; Yates, J. T., Jr.; Bronikowski, M. J.; Huffman, C. B.; Liu, J.; Smalley, R. E.; Hwu, H. H.; Chen, J. G. *J. Am. Chem. Soc.* **2001**, *123*, 10699–10704.

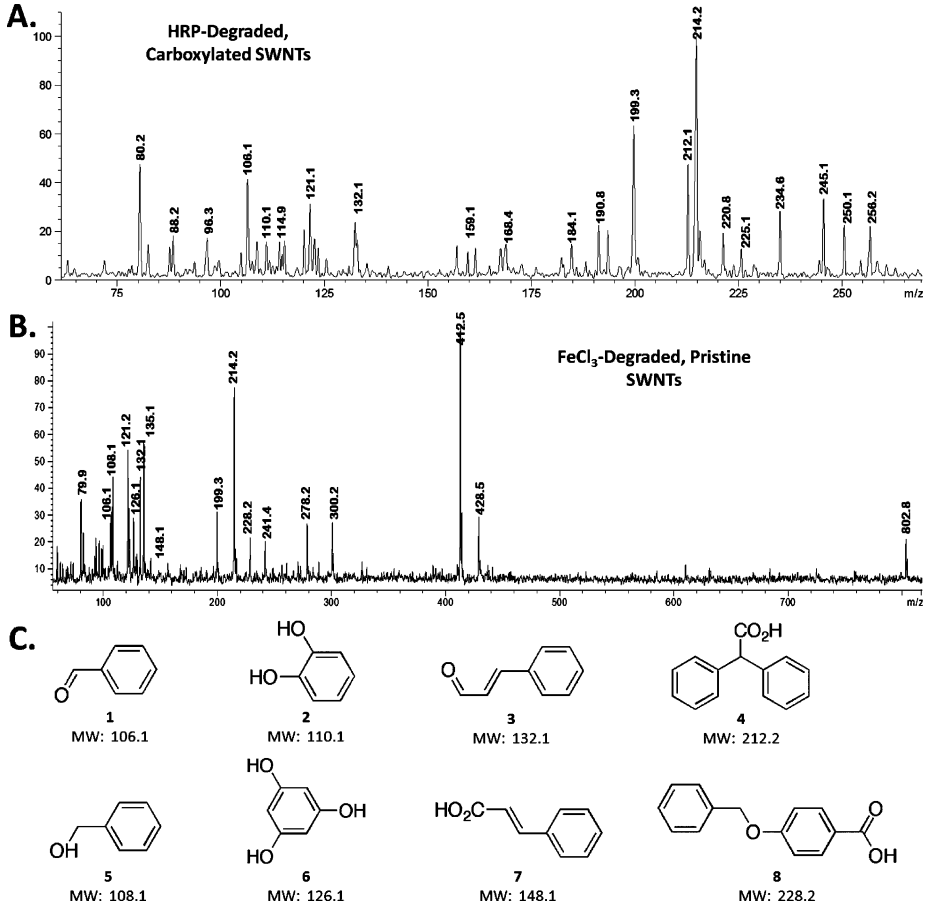

Figure 6. (A) LC−MS spectrum of HRP-degraded, carboxylated SWNTs and (B) $FeCl_3$-degraded pristine SWNTs. (C) Products identified and present in the HRP degradation method included oxidized PAHs such as benzaldehyde (**1**), 1,2-benzenediol (**2**), cinnamaldehyde (**3**), and diphenylacetic acid (**4**). $FeCl_3$-degraded pristine SWNTs produced benzyl alcohol (**5**), 1,3,5-benzenetriol (**6**), cinnamic acid (**7**), and 4-benzyloxybenzoic acid (**8**), as well as products common to both methods (**1** and **3**).

hydrocarbons (PAHs) may be found, suggest the nonspecific oxidation of SWNTs (by hemin and $FeCl_3$) into larger flakes through an "unzipping" effect as opposed to that of HRP degradation, where oxidation is mediated on site-specific areas consistent with TEM observations. Additional structure elucidation of the intermediate degradation products would require their isolation on a preparative scale HPLC and characterization by NMR and mass spectrometry methods, as we are examining a mixture of intermediate products without finite separation.

To identify types of products resulting from the degradation of SWNTs by HRP, hemin, or $FeCl_3$, LC−MS was performed. Briefly, samples were prepared by removing 3 mL aliquots from bulk aqueous solutions, acidifying with 0.1 M HCl, and extracting with dichloromethane (3 mL). After solvent removal, the products were redispersed into 500 μL of MeOH and separated/analyzed using a reversed-phase C18 column and mass spectrometer with conditions identical to those mentioned previously for HPLC. By analyzing positive ions, multiple products were identified from HRP-degraded, carboxylated SWNTs. Shown in Figure 6A, mass to charge (*m*/*z*) values of 106.1, 110.1, 132.1, and 212.1 were observed for HRP-degraded SWNTs, indicative of benzaldehyde (**1**), 1,2-benzenediol (**2**), cinnamaldehyde (**3**), and diphenylacetic acid (**4**). Of significance, $FeCl_3$-degraded pristine SWNTs exhibited similar degradation products (Figure 6B). In addition to those molecules attributed to HRP degradation, benzyl alcohol (**5**), 1,3,5-benzenetriol (**6**), cinnamic acid (**7**), and 4-benzyloxybenzoic acid (**8**) were also identified. This again confirms the presence of similar classes of compounds for both heterolytic and homolytic degradation mechanisms; however, it is important to note that mass spectrometry cannot distinguish between molecular ions and fragments, and preparative scale experiments involving product separation still need to be performed. Moreover, the identified products were similar to those observed in studies of the bioremediation of polycyclic aromatic hydrocarbons (PAHs).[41] In that work, degradation was observed by the addition of cytochrome P_{450} monoxygenase enzyme; PAHs were first oxidized to arene oxides followed by the formation of dyhydrodiols and phenols, as well as aromatic carboxylic acids.[42] Complete oxidation in that case resulted in the formation of CO_2.

As a result of complete oxidative degradation of SWNTs, however, one would expect the final product to be carbon dioxide, a gas. To verify the production of CO_2 as a product of complete degradation, GC−MS was used to analyze the headspace of the sample. As was previously noted, sample vials were prepared by capping with a septum and parafilm, thus allowing for the sampling of headspace using a gastight needle. Approximately 2 μL of sample headspace was injected at two discrete times: (i) prior to the introduction of H_2O_2 to initiate the reaction and (ii) after 10 days of incubation with HRP and

(41) Bamforth, S. M.; Singleton, I. *J. Chem. Technol. Biotechnol.* **2005**, *80*, 723–736.

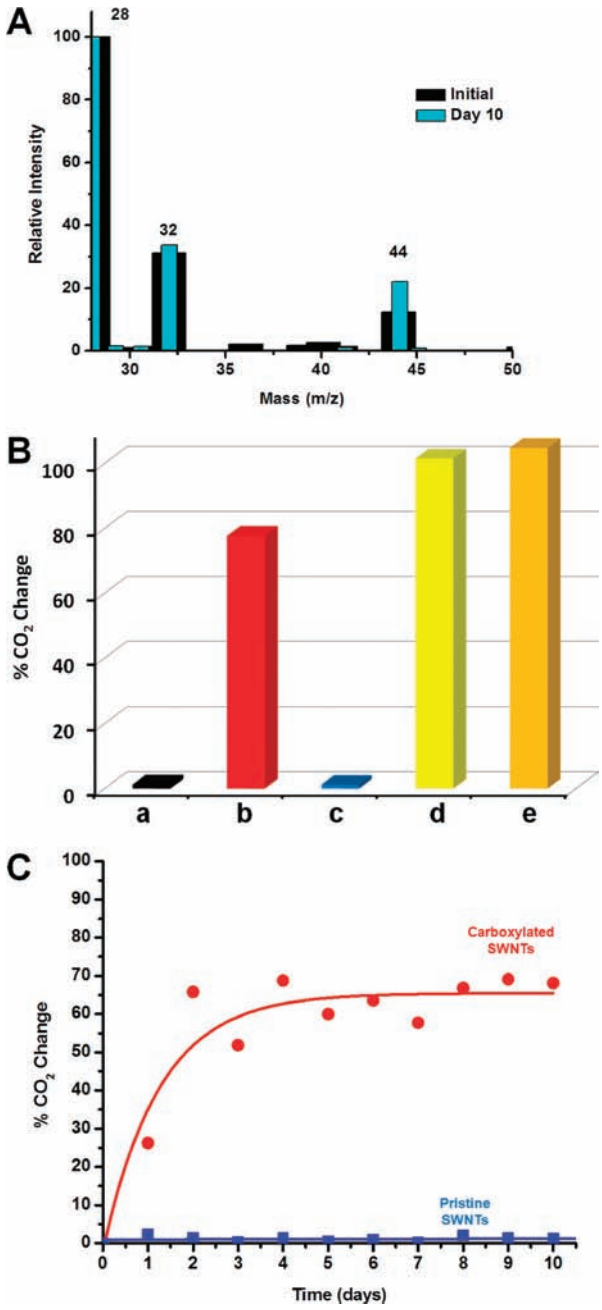

Figure 7. (A) Relative intensity versus mass (*m*/*z*) for CO_2 headspace concentration relative to N_2 for HRP-degraded SWNTs. Enzymatic degradation results in an approximate doubling of the CO_2 concentration. (B) Percent (%) change in the headspace CO_2 concentration after 10 days of incubation of (b) carboxylated SWNTs, HRP, and H_2O_2, (c) pristine SWNTs, HRP, and H_2O_2, (d) carboxylated SWNTs, hemin, and H_2O_2, and (e) carboxylated SWNTs, $FeCl_3$, and H_2O_2. A control of H_2O with daily additions of H_2O_2 (without HRP) is shown in black (a). (C) Kinetics tracking of CO_2 evolution by GC−MS over a 10 day period for carboxylated and pristine SWNTs incubated with HRP and H_2O_2 (800 μM).

H_2O_2. CO_2 concentrations were evaluated relative to ambient N_2 concentrations present in the headspace. Further, a control of double-distilled water and H_2O_2 (no HRP) was treated and analyzed under the same conditions to verify contributions from any possible ambient CO_2 (Supporting Information). Figure 7A demonstrates the increase in CO_2 (*m*/*z*: 44) contributions after 10 days of incubation. Apparently, the abundance of CO_2 doubled over the course of 10 days. Further examination of CO_2 production with hemin and $FeCl_3$-mediated degradation was also performed. The change in the CO_2 abundance after 10 days of SWNT degradation relative to the original value is shown in Figure 7B. As can be seen, the CO_2 concentration became approximately 100% higher with carboxylated SWNTs degraded in the presence HRP, hemin, or $FeCl_3$. Conversely, pristine SWNTs incubated with HRP had a minimal evolution of CO_2, comparable to the control of H_2O. Pristine SWNTs incubated with hemin or $FeCl_3$, however, displayed a marked increase in CO_2 (Supporting Information).

Furthermore, we have monitored the evolution of CO_2 gas in sample headspace on a daily basis to compare the kinetics of the degradation process between carboxylated and pristine SWNTs incubated with HRP and H_2O_2 (800 μM). As shown in Figure 7C, CO_2 evolution was followed for 10 days and measured relative to N_2. As evident from this figure, pristine SWNTs incubated with HRP and H_2O_2 did not produce any significant concentrations of CO_2 in the sample headspace over the course of 10 days, further indicating a lack of degradation of the pristine material. Conversely, when carboxylated SWNTs were incubated with HRP and H_2O_2, CO_2 was measured in the sample headspace and found to follow pseudo first-order kinetics (Figure 7C).

AFM Characterization. Atomic force microscopy (AFM) was used to probe the interaction between HRP and carboxylated SWNTs. Previously, AFM has been implemented to monitor interactions between biological species and SWNTs.[43−46] As such, multiple samples including HRP, carboxylated SWNTs, and HRP incubated with carboxylated SWNTs were imaged in tapping mode using a super sharp silicon probe (<5 nm radius, AppNano). Figure 8A illustrates the height profile of a single HRP molecule. Of important note, because tapping mode was used for imaging, distortions arose in the sample in the form of exaggerated size features.[47] Thus, it was important to perform a cross-section analysis on all samples to verify true height profiles. HRP then demonstrated a height of approximately 5 nm as shown by the section analysis (Supporting Information). Further, Figure 8B shows the height profile of a single, carboxylated SWNT prior to incubation with HRP. Section analysis confirmed a height of 1.8 nm, representative for this type of SWNT (Supporting Information). Upon examining carboxylated SWNTs incubated with HRP (Figure 8C), it was evident that enzyme attachment presumably occurred at the carboxylated sites along the axis of SWNTs. Section analysis (Figure 8D) confirmed this additive effect of enzyme attachment. A similar trend, however, was noted for pristine SWNTs incubated with HRP. AFM of pristine SWNTs interacting with HRP displayed similar enzyme adsorption (Supporting Information). It may be that specific orientations between enzymes and SWNTs in solution promote or inhibit their degradation. Because pristine nanotubes are prone to bundle in solution, it may be that access is limited to the HRP active

(42) Kanaly, R. A.; Harayama, S. *J. Bacteriol.* **2000**, *182*, 2059–2067.
(43) Hafner, J. H.; Cheung, C.-L.; Woolley, A. T.; Lieber, C. M. *Prog. Biophys. Mol. Biol.* **2001**, *77*, 73–110.
(44) McAllister, C.; Karymov, M. A.; Kawano, Y.; Lushnikov, A. Y.; Mikheikin, A.; Uversky, V. N.; Lyubchenko, Y. L. *J. Mol. Biol.* **2005**, *354*, 1028–1042.
(45) Singh, K. V.; Pandey, R. R.; Wang, X.; Lake, R.; Ozkan, C. S.; Wang, K.; Ozkan, M. *Carbon* **2006**, *44*, 1730–1739.
(46) Sano, M.; Kamino, A.; Shinkai, S. *Angew. Chem., Int. Ed.* **2001**, *40*, 4661–4663.
(47) Radmacher, M.; Tillamnn, R. W.; Fritz, M.; Gaub, H. E. *Science* **1992**, *257*, 1900–1905.

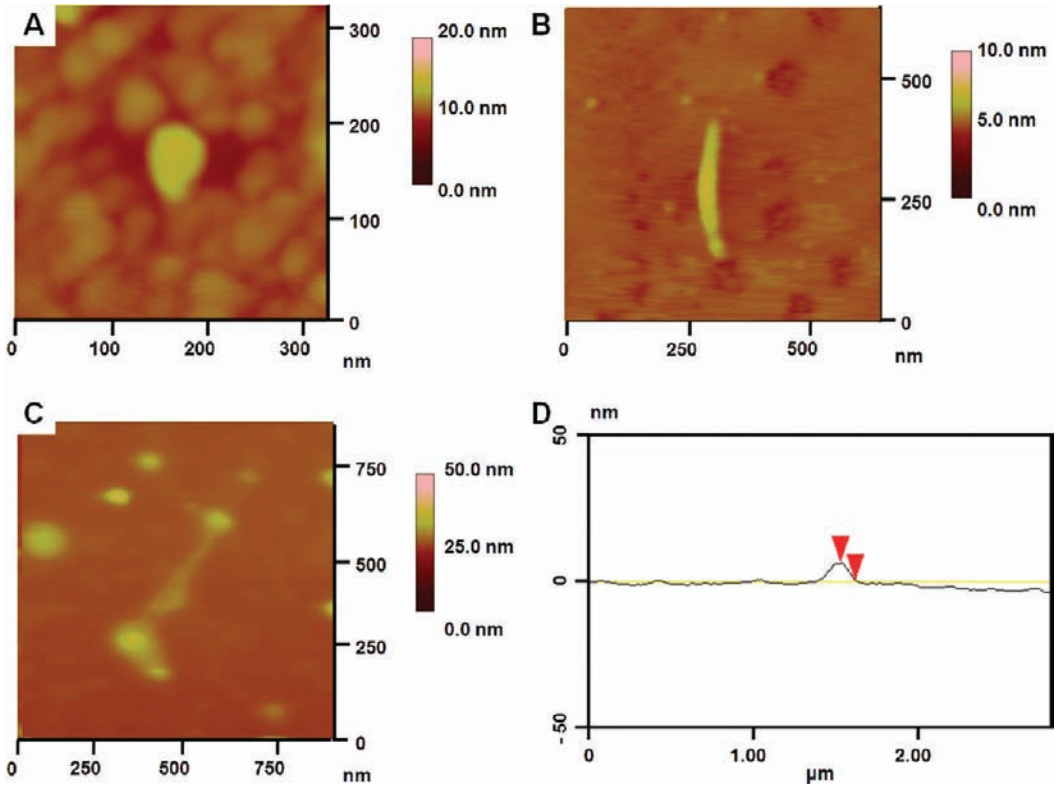

Figure 8. (A) AFM image of single HRP unit under tapping mode imaging. (B) AFM image of single, carboxylated SWNT. (C) AFM image of carboxylated SWNT interacting with multiple HRP units. (D) AFM section analysis of combined carboxylated SWNT and HRP showing a height of approximately 6.0 nm.

site. However, previous high-resolution TEM imaging shows exfoliation of larger bundles near the ends. These sites would then be suitable for enzymatic docking and subsequent degradation. Thus, a more probable scenario would be the docking of pristine SWNTs to an alternative hydrophobic site, further separated from the heme active site responsible for oxidation.

As further proof of proximity effects, carboxylated SWNTs were cast onto a quartz substrate and subjected to identical conditions involving HRP and H_2O_2. Thin-film UV−vis−NIR absorption spectroscopy data suggest that no significant degradation of the SWNT film occurred over a period of 10 days, presumably due to lack of mobility and spatial confinement of carboxylated SWNTs and adsorbed HRP (Supporting Information).

Molecular Modeling. Molecular modeling tested these theories regarding orientation effects between carboxylated and pristine nanotubes with HRP. Suggested previously,[48−50] there is a strong interaction between SWNTs and proteins due to the attractive forces between the carboxyl groups of SWNTs and positively charged domains of proteins. Such adsorption allows for the distance separation of the HRP active site to be diminished in relation to the carboxylated SWNT substrate. By bringing carboxylated SWNTs in proximity to the heme site forming Compound I, it is possible for the reactive species to oxidize and thus degrade SWNTs. It can then be assumed that because of the hydrophobic nature of pristine SWNTs, HRP is forced to align itself in such a way as to result in the increased proximal distance between the heme active site and SWNT substrate. Such a slight increase in distance will discourage the oxidation and thus the degradation of pristine SWNTs. To further understand the molecular interactions during the degradation of modified (carboxylated and hydroxylated) SWNTs by HRP, we identified the possible binding sites on the enzyme to accommodate SWNTs.[51,52] The generated modified and pristine SWNT models with the chirality (8,8), which are metallic SWNTs with 1.3 nm diameters, were docked to the HRP crystal structure (PDB ID: 1H5A, chain A). In each case, the resulting nine complexes were further analyzed to find the best docked conformation. For modified SWNTs with both carboxyl and hydroxyl groups added at the end, 6 out of 9 docked conformations were predicted to bind to HRP in close proximity to the heme binding pocket (Figure 9A,C). The carboxylated ends of the SWNT are oriented toward a positively charged arginine residue, Arg178, on HRP (Figure 9C, Arg is colored in yellow). This may be important in stabilizing the binding of carboxylated/hydroxylated SWNTs with the protein. Analysis of the residues located within 5 Å distance from the docked modified SWNT revealed the presence of F68, N135, L138, A140, P141, F142, F143, T144, Q147, R178, F179, D182, N186, F187, S188, N189, and Q245. The involvement of most of these residues in the catalysis of oxidation reactions has been demonstrated

(48) Kam, N. W. S.; Dai, H. *Phys. Status Solidi B* **2006**, *243*, 3561–3566.
(49) Lee, Y.-M.; Kwon, O.-Y.; Yoon, Y.-J.; Ryu, K. *Biotechnol. Lett.* **2006**, *28*, 39–43.
(50) Davis, J. J.; Coleman, K. S.; Azamian, B. R.; Bagshaw, C. B.; Green, M. L. H. *Chem.-Eur. J.* **2003**, *9*, 3732–3739.
(51) Goodsell, D. S.; Morris, G. M.; Olson, A. J. *J. Mol. Recognit.* **1996**, *9*, 1–5.
(52) Österberg, F.; Morris, G. M.; Sanner, M. F.; Olson, A. J.; Goodsell, D. S. *Proteins* **2002**, *46*, 34–40.

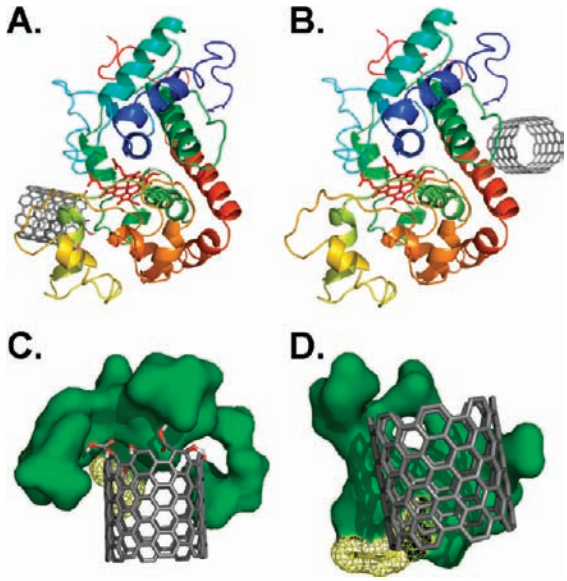

Figure 9. Binding of modified (carboxylated and hydroxylated) and pristine SWNT to horseradish peroxidase. Location of the most preferred binding site on HRP for (A) modified SWNT and (B) pristine SWNT. The corresponding 5 Å binding site residues from the (C) modified SWNT and (D) pristine SWNT to HRP for the predicted binding site locations shown in (A) and (B), respectively. SWNT is colored in gray and rendered in sticks. Residues that correspond to arginine are colored in yellow. The heme is rendered as sticks and colored in red and render as mesh.

previously.[53,54] In addition to this, some of these residues are also part of the catalytically active site of the enzyme.[54] In contrast, for pristine SWNTs, the most preferred interaction site (9 out of 9 conformations) was located at the distal end of the enzyme, opposite from its heme moiety (Figure 9B,D). While the predicted interaction energies for the modified and pristine SWNTs were −15.1 kcal/mol (at the heme binding site) and −15.7 kcal/mol (at the distal end of the heme binding pocket), respectively (Supporting Information), the remoteness of the binding site for pristine SWNTs from the heme makes its catalytic oxidation unlikely. These predictions are in good agreement with the experimental results. Additional controls were performed to examine the effect of sidewall defects on HRP binding, the binding of bundled-pristine SWNTs to HRP, and a comparative inquiry of nanotube chirality where different helicities ((8,8) and (14,4) for metallic and semiconducting nanotubes, respectively) but identical diameter were studied. All results confirmed previous observations and can be found in the Supporting Information. Such data suggest that helicity has no apparent role over preferential enzymatic degradation. Most likely, diameter and especially surface functionalities are responsible for successful oxidation to occur.

Conclusion

Both pristine and carboxylated SWNTs were explored in terms of their ability to degrade in the presence of HRP. Moreover, varying conditions including temperature and concentrations of H_2O_2 were explored. Data suggest that strong adsorption of HRP to carboxylated sites facilitates the degradation of carboxylated SWNTs, while the hydrophobic nature of pristine SWNTs forces HRP to orient in a way that increases the distance between the heme active site and the SWNT surface, thus mitigating the enzyme's oxidative effects. Such data suggest heterolytic cleavage of H_2O_2 to form Compound I, as opposed to homolytic cleavage facilitated by hemin and $FeCl_3$. Use of either of the latter two species catalyzes the homolytic cleavage of H_2O_2, thus forming hydroxyl and hydroperoxyl radicals in a process known as Fenton's catalysis. Moreover, hydroxyl and hydroperoxyl radicals are able to diffuse in solution once formed, and oxidize both carboxylated and pristine SWNT substrates, causing their degradation. Further, the nature of the degradation products has been estimated by HPLC and LC−MS, and the formation of carbon dioxide was established by GC−MS. Future studies involving the preparative scale investigations of products formed during incomplete degradation could reveal their exact structures.

Acknowledgment. This work was supported by AFOSR, Grant no. FA 9550-09-1-0478; NIOSH OH008282 and the 7th Framework Programme of the European Commission (NANOMMUNE).

Supporting Information Available: Amplex Red controls with 80 μM (Figure S1) and 800 μM (Figure S2) H_2O_2 in H_2O, GC−MS control with H_2O (Figure S3), GC−MS of pristine SWNTs and hemin (Figure S4), GC−MS of pristine SWNTs and $FeCl_3$ (Figure S5), HPLC chromatograms of HRP-degraded SWNTs (Figure S6), *trans*-cinnamaldehyde (Figure S7), and mellitic acid (Figure S8), HPLC chromatogram of nonconcentrated sample (Figure S9), HPLC chromatogram of HRP (Figure S10), section analysis of HRP (Figure S11), carboxylated SWNT (Figure S12), and carboxylated SWNT with HRP (Figure S13), AFM image of pristine SWNTs (Figure S14), section analysis of pristine SWNTs (Figure S15), AFM image of pristine SWNTs and HRP (Figure S16), section analysis of pristine SWNTs and HRP (Figure S17), UV−vis−NIR spectra of carboxylated SWNTs on fixed substrate (Figure S18), carboxylated SWNTs degraded by hemin (Figure S19), carboxylated SWNTs degraded by $FeCl_3$ (Figure S20), EDXA of products from pristine SWNTs degraded by hemin and H_2O_2 (Figures S21, S22), intermolecular binding energies (Figure S23), molecular modeling of HRP interaction with sidewall defects (Figure S24), interaction of HRP with bundled pristine SWNTs (Figure S25), and a comparative study of HRP docking with varying chirality SWNTs (Figure S26). This material is available free of charge via the Internet at http://pubs.acs.org.

JA9083623

(53) Das, P. K.; Caaveiro, J. M. M.; Luque, S.; Klibanov, A. M. *J. Am. Chem. Soc.* **2002**, *124*, 782–787.
(54) Henrikson, A.; Schuller, D. J.; Meno, K.; Welinder, K. G.; Smith, A. T.; Gajhede, M. *Biochemistry* **1998**, *37*, 8054–8060.